A Two-Dimensional Approach to Rubber V-Belt Mechanics

Francesco Sorge

***Abstract*— A new two-dimensional approach to the mechanics of rubber V-belt CVT's takes into account the change, along the belt sides, of the sliding velocity on the pulley walls, together with the cross section rotation due to the shear forces. The results show significant differences with the one-dimensional thin belt model and point out the gradual increase or decrease of the belt curvature in the entrance and exit regions of the contact arc, which implies the negligibility of the belt arching in the free spans. Some experimental tests on the global variables of a rubber belt CVT indicate a very fine acceptability of the theoretical model.**

I. Introduction

RUBBER V-Belt CVT's with short center distances and different winding arcs require high adherence properties at the belt-pulley contact, as the belt flexural stiffness tends to arch the belt line in the free strand and reduce the contact width. Nevertheless, this arching is compensated in part by the belt softening due to the shear deflection and by the transverse compliance, which produces a gradual penetration into the groove. The shear force and deformation in the free span may become important near the boundary with the wrap arc, influencing the variables of the belt-pulley coupling (tension, penetration, sliding angle) up to some distance from the contact endpoints [1]-[3]. The present approach addresses these effects and formulates a new two-dimensional model for the steady V-belt mechanics, extendable to the shift phases as well.

The belt is considered as a slender ring-beam, whose external surface forms a closed stream tube where a continuous material flows inside. The Reynolds transport theorem is applied to the mass and momentum fluxes through a fixed elementary control volume. The Timoshenko beam approach is used in the analysis of the belt deflection, including the shear deformation. The contact wall forces are assumed variable, in both strength and direction, along the sides of the belt cross-section because of the variation of the local velocities of the pulley plates and of the belt. Actually, the local sliding velocities, and hence the friction forces, depend on the belt penetration angle, on the radial coordinate, on the distance from the belt centre of curvature, which does not coincide with the pulley centre, and on the change rate of the angle formed by the belt cross-section and the cord layer, which is proportional to the change rate of the shear force.

The differential equations of the dynamical model, which expands the analysis of [4], will then specify the geometrical configuration of a belt path segment, the mass conservation, the equilibrium of a belt element in the directions parallel and normal to the belt, the rotational equilibrium, the constitutive elastic properties of the belt in the axial direction and the elastic belt deflection. The model is considered valid for either the wound region or the free strands, including or ignoring the side forces.

Experimental tests are carried out on a rubber V-belt CVT, using the test bench described in [5]. The simulation of the belt behaviour by the present model is shown to give a quite good accordance with the experimentation.

Francesco Sorge is with the Department of Mechanics, University of Palermo, 90128 – Palermo, Italy (phone: +39 091 6657157; fax: +39 091 6657163; e-mail: sorge@dima.unipa.it).

II. Theoretical Model

All physical quantities will be supposed uniformly distributed along the transverse (axial) direction, so that any three-dimensional effect will be ignored. Reference is made to Fig. 1-3 for the notation.

A. Free Strand Analysis

No surface forces act on the belt sides and the one-dimensional analysis of references [1]-[3] may be correctly applied, as summarized hereafter, assuming that the belt deformation remains within the field of linear elasticity.

The seating and unseating boundary points are indicated with B, the slack and tight spans with the subscripts $\ldots_S$ and $\ldots_T$, the driver and driven pulleys with the subscripts $\ldots_R$ and $\ldots_N$. The example reference frame (B_{RT},x,y) of Fig. 1 has its x axis parallel to the ideal geometric tangent to both pulleys and another frame (B_{RS},x,y) may be similarly introduced at the boundary point B_{RS}, with the x axis directed towards the driven pulley and the y axis towards the driver pulley inside.

Considering an elementary control volume between two fixed cross-sections distant dc and balancing the momentum flux with the external forces, one gets $d[(N-\mu v^2)\mathbf{t}]/dc + d(S\mathbf{n})dc = 0$, where μ and v are the unit length mass and the belt velocity (see detail of Fig. 1). The belt inertia is thus associated with the tensile force N by defining the "dynamic" tension and the "dynamic" elongation, $T = N - \mu v^2$ and $\varepsilon = T/S_l$, where S_l is the longitudinal stiffness. The rotational equilibrium gives $dM + Sdc = 0$.

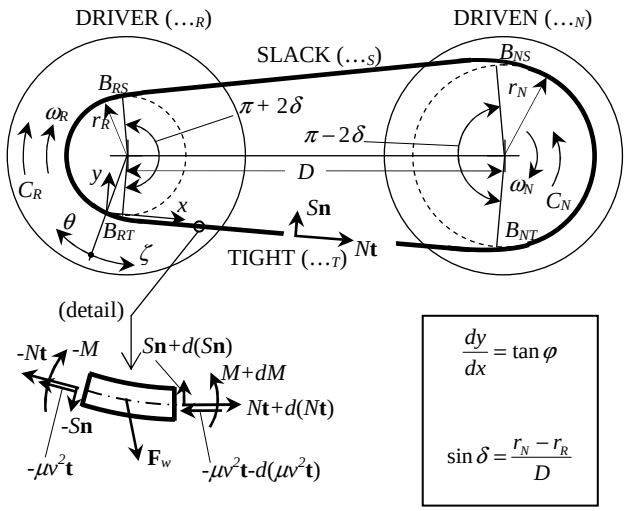

Fig. 1. Scheme of belt drive. For …$_I$ = …$_R$ or …$_N$ and …$_J$ = …$_T$ or …$_S$, B_{IJ} = boundary points of contact regions; C_I = torque; ω_I =angular speed.

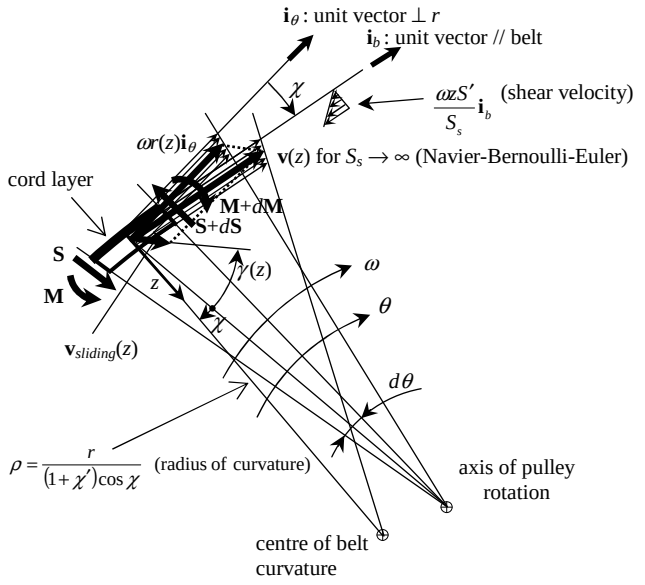

Fig. 2. Velocity distribution across the belt thickness. Primes: derivatives with respect to θ; z :coordinate normal to the cord layer; $\gamma(z)$ = sliding angle in rotation plane; χ = penetration angle; S_s = shear stiffness [N].

Introducing the shear ratio $\tan\psi = S/T$ and the belt slope $\varphi = \arctan(dy/dx)$, integrating the two scalar components of the equilibrium equation and using the generic subscript …$_J$ for …$_T$ or …$_S$, one obtains $T(\varphi) = T_{RJ}\cos(\varphi - \varphi_{RJ} - \psi_{RJ})/\cos\psi_{RJ}$ and $S(\varphi) = -T_{RJ}\sin(\varphi - \varphi_{RJ} - \psi_{RJ})/\cos\psi_{RJ}$, whence $S = dT/d\varphi$, $T = -dS/d\varphi$. The shear force vanishes for $\varphi = \varphi_{RJ} + \psi_{RJ}$ and is positive or negative on the driver or driven side of this section.

Defining the flexural stiffness and the shear stiffness with S_f and S_s, indicating the original factory radius with $r_{fact.} = l_{belt}/2\pi$, the belt deflection equation is $d\varphi/dc - 1/r_{fact.} = M/S_f + (dS/dc)/S_s$, which gives by differentiation and by use of the rotational equilibrium

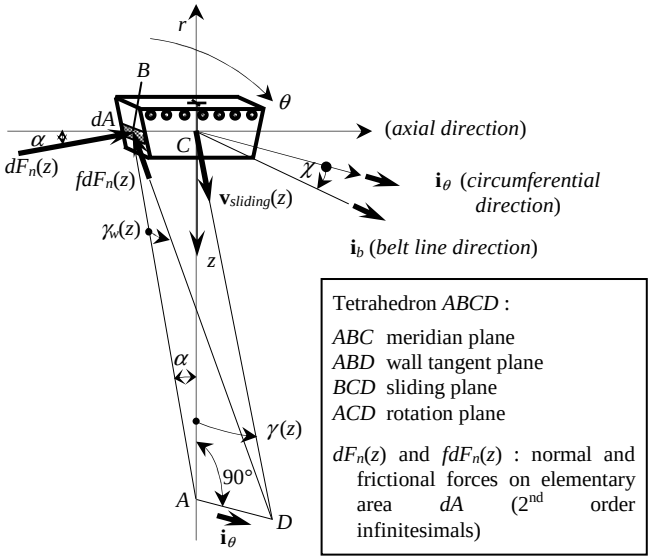

Fig. 3. Wall forces on belt element. f = coefficient of friction; α = groove half-angle; $\gamma_w(z) = \arctan[\cos\alpha\tan\gamma(z)]$ = sliding angle on pulley wall.

condition and the above relationships between T and S:

$$\left(1+\frac{T}{S_s}\right)\frac{d^2\varphi}{dc^2}+\frac{S}{S_f}\left[1+\frac{S_f}{S_s}\left(\frac{d\varphi}{dc}\right)^2\right]=0 \qquad (1)$$

Introducing the small flexural parameter $P = S_f/D^2S_l$, which is of order $O(1/10000 \div 1/500000)$ for rubber V-belts reinforced by embedded cords, and the longitudinal-to-shear stiffness ratio $s = S_l/S_s$, which is usually rather large because of the high cord stiffness, the following orders of magnitude are to be presumed: $\varepsilon = O(\sqrt{P})$, $\varphi_{IJ} = O(\sqrt[4]{P}) = O(\sqrt{\varepsilon})$, $\psi_{RJ} = O(\sqrt[4]{P})$, $s \cong O(1/\sqrt{P}) = O(1/\varepsilon)$.

Using the dimensionless co-ordinate $\zeta = c/D$, variable between 0 and $c_{\max.}/D \approx \cos\delta$, Equation (1) may be written in the form $sP(d^2\varphi/d\zeta^2)/[1 + sP(d\varphi/d\zeta)^2] + s(d\varepsilon/d\varphi)/(1 + s\varepsilon) = 0$, so that a first integration can be worked out exactly and leads to $(1 + s\varepsilon)^2/[1 + sP(d\varphi/d\zeta)^2] = \text{constant} = (1 + s\varepsilon_{RJ})^2/[1 + sP(d\varphi/d\zeta)_{RJ}^2]$.

A second integration may be carried out by separation of the variables and, taking into consideration the above orders of magnitude, may be calculated as in [3] in the approximate form $\varphi = \varphi_{RJ}\cosh(\Omega\zeta) + (d\varphi/d\zeta)_{RJ}\sinh(\Omega\zeta)/\Omega$, where $\Omega = 1/\sqrt{P(s+1/\varepsilon_J)}$ is a quite large parameter, whence it is expected that $\varphi_{RJ} \cong -(d\varphi/d\zeta)_{RJ}/\Omega$ and φ is very small almost everywhere along the free span save in the neighbourhoods of the two endpoints. Moreover, ψ_{RJ} turns out to be nearly equal to $-\varphi_{RJ}$.

Imposing the end condition for the slope and the curvature at the boundary points with the driven pulley, one gets as in [3]

$$\varphi_{RJ} \cong -\frac{1}{\Omega}\left(\frac{d\varphi}{d\zeta}\right)_{RJ} \cong -\psi_{RJ} \qquad \varphi_{NJ} \cong +\frac{1}{\Omega}\left(\frac{d\varphi}{d\zeta}\right)_{NJ} \cong -\psi_{NJ} \quad (2a,b)$$

Comparing with the conventional arching model [6], where the Navier bending theory is applied and $|\varphi_{IJ}| = \sqrt{P/\varepsilon_J}\ (D/r_{I,\infty})$, the loss of the contact angle is quite smaller, due to the fact that $|(d\varphi/d\zeta)_{IJ} << (D/r_{I,\infty})$ because of the gradual increase of the belt curvature towards the inside of the boundary region of the contact arc.

B. Analysis of the Contact Region

The one-dimensional model of references [1] to [5] is here refined taking into account the variation, along the sides of the belt cross-profile, of the sliding velocity on the pulley wall. The cord layer is assumed on the top and is considered as the neutral layer due to its much higher longitudinal stiffness with respect to the rubber. The coordinate z is measured from the cord, orthogonally to it as in Fig. 2. No hunching is supposed for the cross section, which is assumed to remain plane and rotate with respect to the cord because of the shear force.

Indicate with $\bar{r}$ the radial coordinate of the top cord and with $x = (r_\infty - \bar{r})/r_\infty$ the dimensionless elastic penetration, where r_∞ is the radius for infinite transverse stiffness, so that $\bar{r} = r_\infty(1-x)$. The geometrical condition $\bar{r}' = -\bar{r}\tan\chi$ may be turned into the dimensionless form

$$x' = (1-x)\tan\chi \qquad (3)$$

Applying Carnot's theorem, the pulley velocity varies with z according to $\omega r(z) = \omega\sqrt{\bar{r}^2 - 2z\bar{r}\cos\chi + z^2} \cong \omega r_\infty(1 - x - ZH\cos\chi)$, where $Z = z/h$ is a dimensionless coordinate, variable between 0 and 1, h is the belt thickness and $H = h/r_\infty$ (<< 1).

Likewise, the velocity of the belt side points can be thought as composed of a "rigid" rotation around the centre of curvature and of a shear rotation around the top cord (see Fig. 2). Ascribe the longitudinal belt force to the only cord layer, which is much stiffer than the rubber and apply the mass conservation condition to such a layer as in the one-dimensional model: $\bar{v} = v_\infty(1+\varepsilon)$, where the subscript ∞ refers to an infinite longitudinal stiffness. Then, it is possible to write $v(Z) = v_\infty(1+\varepsilon)[1 - ZH\cos\chi(1+\chi')/(1-x)] - \omega r_\infty HZs\sigma'$, where $\cos\chi(1+\chi')/\bar{r}$ is the belt cord curvature and $\sigma = S/S_l$ is the dimensionless shear force.

The generic triangle of velocities of Fig. 2 indicates that $v\cos\chi - \omega r = v\sin\chi\tan\gamma$ and, using the above results and neglecting small order terms, one gets a two-dimensional relationship for the sliding angle $\gamma(Z)$

$$\tan\gamma(Z) = \frac{1}{\tan\chi}\left\{1-\kappa\frac{(1-x)\left[1-\frac{ZH\cos\chi}{(1-x)}\right]}{\cos\chi(1+\varepsilon)\left[1-\frac{ZH\cos\chi(1+\chi')}{(1-x)}-\kappa\frac{ZHs\sigma'}{(1+\varepsilon)}\right]}\right\} \cong \quad (4)$$
$$\cong \frac{1}{\tan\chi}\left\{1-\kappa\frac{(1-x)[1+ZH(\chi'+s\sigma')]}{\cos\chi(1+\varepsilon)}\right\}$$

where $\kappa = \omega r_\infty/v_\infty \cong 1$ is a constant kinematic parameter, which is calculable in dependence on the variable values at some specific point of the wrap arc (e.g. the exit point).

The vectorial equilibrium equation is similar to the free strand, but considering also the wall force vector ($\mathbf{F}'_w$ per unit angle), whose components are calculable by summing the effects of the elementary compression and friction forces acting on the various stripes dA of Fig. 3:

$$(dF'_w)_{//\text{ belt}} = 2dF'_n \times \times[\sin\alpha\sin\chi + f(\cos\gamma_w\cos\alpha\sin\chi + \sin\gamma_w\cos\chi)] \quad (5)$$

$$(dF'_w)_{\perp\text{ belt}} = 2dF'_n \times \times[\sin\alpha\cos\chi + f(\cos\gamma_w\cos\alpha\cos\chi - \sin\gamma_w\sin\chi)] \quad (6)$$

where $\gamma_w(Z) = \arctan(\cos\alpha\tan\gamma)$ indicates the sliding angle on the tangent plane, function of Z (Fig. 3).

Assume an elastic modulus E_{axial} in the axial direction and suppose it constant across the belt thickness h. Indicating the belt width with $w(Z) = \bar{w}(1 - 2ZW\tan\alpha)$, where $W = h/\bar{w}$ and the over-bar refers to the top cord layer, the axial equilibrium condition may be combined with the belt constitutive properties, giving:

$$(dF'_w)_{\text{axial}} = dF'_n\times(\cos\alpha - f\cos\gamma_w\sin\alpha) = = \frac{2\tan\alpha E_{axial}hr_\infty^2 x(1-x-ZH\cos\chi)}{\bar{w}(1-2ZW\tan\alpha)\cos\chi}dZ = = \frac{kS_l x(1-x-ZH\cos\chi)}{2\tan\alpha\cos\chi(1-2ZW\tan\alpha)}dZ \quad (7)$$

where the belt elastic parameter $k = 4\tan^2\alpha\ E_{axial}\ hr_\infty^2/(\bar{w}\,S_l)$ has been introduced as in [1]-[3], whose value is proportional to the square of the wrap radius on the pulley.

The elementary normal force dF_n must be calculated by (7) as a function of Z and replaced into Eqs. (5-6), which must be integrated from $Z = 0$ to $Z = 1$ to get the wall forces on the belt element in the directions parallel and normal to the belt.

Observing that $d\mathbf{n}/d\theta$ and $d\mathbf{t}/d\theta$ are tangent and orthogonal to the belt respectively and both equal in modulus to the dimensionless curvature $d\varphi/d\theta = d(\theta + \chi)/d\theta = 1 + \chi'$, the corresponding internal force components acting on a belt element through the upstream and downstream cross sections are $dT + S(1+\chi')d\theta$ and $T(1+\chi')d\theta - dS$.

Thus, dividing by $S_l d\theta$, the equilibrium equation can be split in its two components:

$$// \text{ belt}: \quad \varepsilon' + \sigma(1+\chi') = $$
$$= kx(1-x)\int_0^1 \left(\frac{1-\frac{ZH\cos\chi}{1-x}}{1-2ZW\tan\alpha}\right)\left(\frac{\tan\chi+\tan\beta}{1-\frac{\tan\beta}{\cos^2\alpha\tan\gamma}}\right)dZ \qquad (8)$$

$$\perp \text{ belt}: \quad \varepsilon(1+\chi') - \sigma' = $$
$$= kx(1-x)\int_0^1 \left(\frac{1-\frac{ZH\cos\chi}{1-x}}{1-2ZW\tan\alpha}\right)\left(\frac{1-\tan\beta\tan\chi}{1-\frac{\tan\beta}{\cos^2\alpha\tan\gamma}}\right)dZ \qquad (9)$$

where $\tan\beta = f\sin\gamma_w/(\sin\alpha + f\cos\gamma_w\cos\alpha)$ and $\beta = \beta(Z)$.

Recalling the deflection equation, considering that $dc = r_\infty(1-x)d\theta/\cos\chi$, minding the positive increasing direction of the shear force along the arc of contact, different from the free span (Fig. 1), and introducing the dimensionless bending moment variable $m = \left(M/S_f + 1/r_{fact.}\right)r_\infty(1-x)/\cos\chi$, one has

$$m = \varphi' + s\sigma' \qquad \rightarrow \qquad \chi' + s\sigma' = m - 1 \qquad (10)$$

Equation (1) incorporates the deflection equation and the rotational equilibrium condition but refers to the free span and does not take into account the moment of the wall friction forces, which is given by the integral $\int_0^h z\left(dF_w'\right)_{//\text{belt}}d\theta$ and implies writing the rotational equilibrium in the form $dM/dc = S - \int_0^h z\left(dF_w'\right)_{//\text{belt}}\cos\chi/\bar{r}$ for the contact region. Therefore, minding that $dc = \bar{r}\,d\theta/\cos\chi$, whence $d^2(\ldots)/dc^2 = [(\ldots)'' + (\ldots)'(1-\chi')\tan\chi]\cos^2\chi/\bar{r}^2$, Equation (1) can be changed into the dimensionless form

$$m' = m\tan\chi(\chi'-1) + \frac{1}{P}\left(\frac{1-x}{\cos\chi}\right)^2\left[\sigma - \right.$$
$$\left. kHx\cos\chi\int_0^1 Z\left(\frac{1-\frac{ZH\cos\chi}{1-x}}{1-2ZW\tan\alpha}\right)\left(\frac{\tan\chi+\tan\beta}{1-\frac{\tan\beta}{\cos^2\alpha\tan\gamma}}\right)dZ\right] \qquad (11)$$

Equations (3), (4) and (8)-(11) constitute a system of five ordinary differential equations and a parametric equation, Eq. (4), in the six variables x, ε, σ, γ, χ and m. The domain is the whole region of contact and the boundary conditions are given by: (b1-b2) $x = 0$ at the entrance and exit endpoints; (b3-b4) $\varepsilon = \varepsilon_{in}$ and $\varepsilon = \varepsilon_{out}$ at these points, in dependence on the belt forcing and the torque; (b5-b6) the matching of the shear with the tight and slack free spans by Eqs. (2), to be written in the form $\sigma = \pm\sqrt{P\varepsilon(1+s\varepsilon)}\,(1+x'')$ (plus or minus sign for entrance or exit points, see [3]).

This differential system is strongly non-linear and appears of the boundary layer type, that is to say it changes to a lower differential order when neglecting some smaller terms, so that not all the boundary conditions can be fulfilled. Such a "degenerescent" trend is typical of all V-belt models, also in a one-dimensional analysis and/or in the shift phases of CVT's [7]. Nevertheless, it is worsened by the two-dimensional shear effects. The solutions are sought as for an initial value problem, starting from the contact exit point with zero penetration x and integrating by a Runge-Kutta routine as far as the penetration vanishes again, at the contact entrance. The integration is repeated by iterative shooting techniques until all the mentioned boundary conditions are fulfilled.

III. Results. Practical Formulary

Figures 4 and 5 show the numerical solutions for two example cases, of a driver and a driven pulley. The data were chosen according to the characteristics of a small rubber belt CVT, whose tests appear in the next section.

Each figure shows, in the upper side, the diagrams of the dynamic longitudinal elongation $\varepsilon = (N - \mu v^2)/S_l$ of the dimensionless radial penetration $x = \Delta r/r_\infty$ and of the dimensionless shear force $\sigma = S/S_l$. In the lower side, the diagrams of the sliding angle are traced for various distances from the top cord. It is possible to see the significant variability of the sliding conditions on proceeding from the top towards the interior, due to the variation of the pulley and belt velocities along this direction. The whole force on the belt element sides is given by the sum of the small forces on the single longitudinal slices dA and involves significantly different distributions of the belt tension and penetration with respect to the one-dimensional approach of [1]-[7]. On the contrary, the shear force diagram is little affected by the two-dimensionality of the model and turns out to be very similar to ref. [3]. The shear force is much smaller than the belt tension and is in practice negligible in the main inner region of contact. It exhibits a decreasing trend in the seating region and a decreasing-increasing trend with a minimum value in the unseating region.

The lower plots of Figg. 4 and 5 report alos the belt curvature and indicate that it is nearly equal to the ideal wrapping curvature in the main inner region, but is subject to a gradual but rather rapid reduction in the two boundary

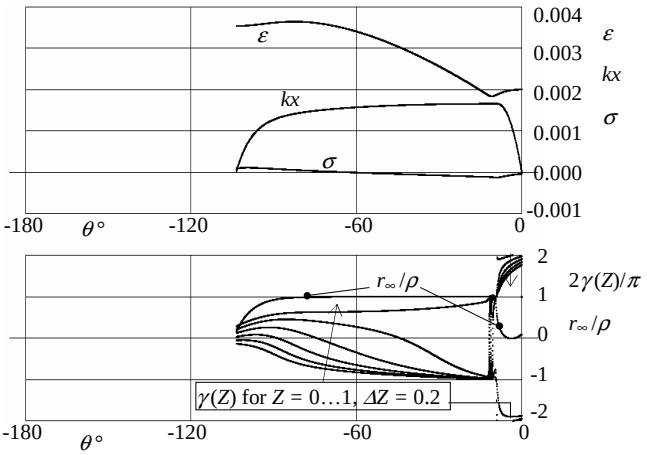

Fig. 4. Example of driver pulley solution.
Data: f = 0.4; k = 0.15; α = 13°; $S_f / (S_l r^2)$ = 0.00004; $\gamma_{out}(0)$ = 191°

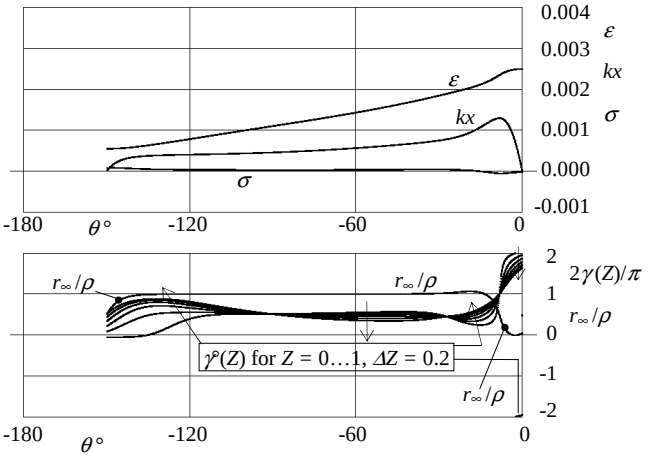

Fig. 5. Example of driven pulley solution.
Data: f = 0.4; k = 0.15; α = 13°; $S_f / (S_l r^2)$ = 0.00004; $\gamma_{out}(0)$ = 184°

regions until becoming quite small at the entrance and exit endpoints.

In addition, through the observation of several solutions curves for the highest torque levels, a simplified heuristic model can be formulated for the axial thrust, which can be helpful for many design problems.

As regards the driver pulleys, the penetration x is rather uniform along the inner region of contact, while it increases in the seating region and decreases in the unseating one with a trend which can be roughly approximated by two parabolic laws. Moreover, the ratio $\xi_R = \varepsilon_{in}/(kx_{inner})$ remain roughly unchanged for several wrap angles and tensioning levels and may be thought to be a characteristic number of each belt drive. A similar conclusion may be approximately derived for the widths of the seating and unseating regions, $\Theta_{R,seat}$ and $\Theta_{R,unseat}$, so that, after estimating these three parameters, ξ_R, $\Theta_{R,seat}$ and $\Theta_{R,unseat}$, the axial thrust calcualtion is very easy for driver pulleys, approximating Eq. (7) with its dominant terms, i. e. $F'_{R,axial} = kxS_l/(2\tan\alpha)$, and integrating with respect to θ.

The driven pulley solutions for x lead to similar approximations, except that they show an increasing trend inside the inner region, according roughly to a monomial power law, and a sort of bump in the unseating region, whose height is roughly given by $kx_{max.} \cong \varepsilon_{out}/2$ (see Fig. 5).

Putting $\ldots_I = \ldots_R$ or $\ldots_N$ (driver or driven) and $\ldots_J = \ldots_T$ or $\ldots_S$ (tight or slack), one has the compact formulation

$$\text{seating} \qquad F'_{I,\text{axial}} = \frac{T_J}{2\xi_I \tan\alpha}\left[1-\left(\frac{\theta}{\Theta_{I,seat}}-1\right)^2\right]$$

$$\text{inner} \quad \begin{cases} F'_{R,\text{axial}} = \dfrac{T_T}{2\xi_R \tan\alpha} \\ F'_{N,\text{axial}} = \dfrac{T_S}{2\xi_N \tan\alpha} + \dfrac{\lambda}{2\tan\alpha}\left(\theta-\Theta_{N,seat}\right)^n \end{cases} \tag{11}$$

$$\text{unseating} \quad F'_{I,\text{axial}} = \frac{T_T}{2\xi_{I,unseat} \tan\alpha}\left[1-\left(\frac{\Theta_I-\theta}{\Theta_{I,unseat}}-1\right)^2\right]$$

where $\ldots_J = \ldots_T$ and $\ldots_S$ for $\ldots_I = \ldots_R$ and $\ldots_N$ respectively, Θ_I is the whole wrap width, $\xi_{R,unseat} = \xi_R$ and $\xi_{N,unseat} = 2$. In the driven pulley case in particular, the coefficient λ is obtainable by connecting the partial diagrams and is given by $\lambda = (0.5T_T - T_S/\xi_N)/(\Theta_N - \Theta_{N,seat} - \Theta_{N,unseat})^n$.

IV. Experimental Comparison

Some experimental results were collected extracting the steady sub-phases from several shift tests carried out on a continuously variable transmission (CVT) using the test bench described in [5].

A DC electric motor drove the transmission, while a pneumatically operated disk brake applied the resistant torque. The continuously variable unit consisted in a small power motorcycle variator with a downstream reduction gearing of ratio 13:1.

The speed and torque were measured on the driver and driven sides by two speed-torque meters of the strain-gauge type and the winding radius changes of both pulleys were measured by two LASER sensors. All electric signals were channelled to a data acquisition system and worked out by special software.

The belt stiffness in the longitudinal and transverse directions was measured on a testing machine giving: S_l = 59000 N, $E_z h/\overline{w}$ = 21 Nmm^{-2}. Load tests on a clamped piece of belt gave the flexural stiffness S_f = 6500 Nmm^2 and the shear stiffness S_s = 105 N. These measures correspond to the data of Figg. 4 and 5, so that the numerical calculation permits estimating the following parameter values, $\Theta_{I,seat} \cong \pi/6$, $\Theta_{I,unseat} \cong \pi/18$, $\xi_R \cong 2.2$, $\xi_N \cong 1.5$, n =

5, whence $\lambda = (0.5T_T - T_S/1.5)/(\Theta_N - 2\pi/9)^5$, and integrating Eqs. (11). Then

$$F_{R,\text{axial}} \cong \frac{T_T}{4.4\tan\alpha}\left(\Theta_R - \frac{2\pi}{27}\right)$$

$$F_{N,\text{axial}} \cong \tag{12a,b}$$

$$\cong \frac{T_S}{3\tan\alpha}\left(\Theta_N - \frac{\pi}{9}\right) + \frac{\pi T_T}{108\tan\alpha} + \frac{(3T_T - 4T_S)}{72\tan\alpha}\left(\Theta_N - \frac{2\pi}{9}\right)$$

The experimental evaluation of the axial thrust was indirect, as it was calculated using the measures of the wrap radii, the knowledge of the operative characteristics of the two actuators and the previous measurement of the actuator parameters. On the driver side, a centrifugal mass system adjusted the speed ratio to the input speed, while on the driven side, a loading spring generated the belt forcing and moreover, the axial thrust was corrected by the resistant torque through a suitable helical shape of the coupling tracks between the movable and fixed half-pulleys.

Considering the torque equation, $T_T - T_S = 0.5\times(C_R/r_{\infty R} + C_N/r_{\infty N})$, it is possible to calculate the tight and slack tension forces, T_T and T_S, by the measures of the driver and driven torque, by the experimental estimation of any one of the two axial forces, e. g. $F_{N,axial}$, based on the actuator characteristics, and by use of the correspondent Eq. (12). Then, the theoretical value of the other axial force, e. g. $F_{R,axial}$, is calculable with the other of Eqs. (12) and comparable with its experimental counterpart.

As an example, Figure 6 shows the results for several test cases and indicate a very fine agreement between the theoretical and experimental values of $F_{R,axial}$, though it is to be emphasized that the approximation, Eqs. (11-12), is based on a global estimation of the axial thrust and does not ensure that the assumed plot of the elastic penetration x conforms exactly to the true situation: other diagrams of x might give the same axial thrust F_{axial}, provided that they subtend the same area.

V. Conclusion

The numerical results of the present analysis show that the trend of most belt variables is somewhat different from the thin belt model with no shear. Moreover, which is quite interesting, the curvature of the belt at the entrance and the exit of the pulley is very small, so that the free span shape is more close to a straight line than to the conventional

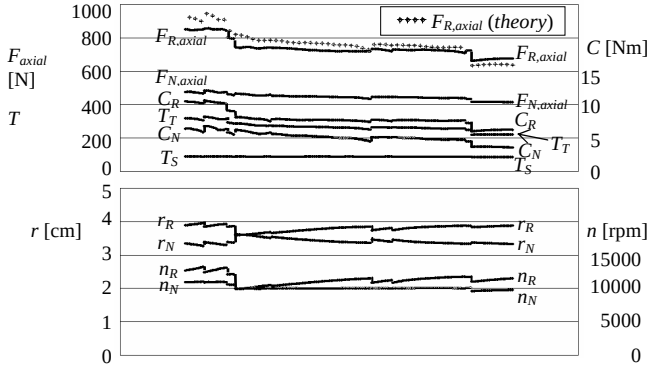

Fig. 6. Comparison between theory and experiments. Measures at successive time instants (abscissae).

Data of CVT:

belt length = 758 mm; centre distance = 255 mm; belt width = 15.5 mm; unit length mass of belt = 0.124 g/mm; groove half-angle = 12.8 deg; belt-pulley coefficient of friction = 0.4

flexural arch. The curvature increases on the contrary towards the inside of the wound arc in the short boundary regions, of seating and unseating, together with the elastic belt penetration inside the groove. Therefore, the conventional belt arching theory overestimates the loss of the arc of contact, which appears nearly inexistent indeed, to some advantage of the gross slip prevention.

References

[1] F. Sorge, "Shear Compliance and Self Weight Effects on Traction Belt Mechanics", *Proc. of the IMechE, Journal of Mechanical Engineering Science, part C*, v. 221, 2007, pp. 1717-1728.

[2] F. Sorge, "A Note on the Shear Influence on Drive Belt Mechanics", *ASME Trans., J. of Mechanical Design*, v. 130, n. 2, 2008, pp. 024502 (1-5).

[3] F. Sorge, "Joint Influence of Transverse Compression and Shear-Flexural Stiffness on Rubber V-Belt Mechanics", *Proc. of the JSME Intern. Conf. on Motion and Power Transmission, MPT 2009*, Sendai, Japan, 13-15/05/2009, pp. 603-608.

[4] G. Gerbert and F. Sorge, "Full Sliding "Adhesive-Like" Contact of V-Belts", *ASME Trans., J. of Mechanical Design*, v. 124, n. 4, 2002, pp. 706-712.

[5] M. Cammalleri and F. Sorge, "Approximate Closed-Form Solutions for the Shift Mechanics of Rubber Belt Variators", *IDETC/CIE 2009, ASME 2009 Intern. Design Engineering Techn. Confer., Computer and Information in Engin. Confer.*, S. Diego, CA (USA), 30/8-2/9 2009.

[6] Gerbert, G., *Traction Belt Mechanics, Flat belts, V-belts, V-rib belts*, Chalmers Tekniska Högskola, Göteborg, Sweden, 1999.

[7] Sorge F., "A Theoretical Approach to the Shift Mechanics of Rubber Belt Variators", *ASME Trans., J. of Mechanical Design*, v. 130, n. 12, 2008, pp. 122602 (1-9).